Supporting Information for

Tracking Photoinduced Au-Au Bond Formation through Transient Terahertz Vibrations Observed by Femtosecond Time-Domain Raman Spectroscopy

Hikaru Kuramochi[1,2,3], *Satoshi Takeuchi*[1,2], *Munetaka Iwamura*[4], *Koichi Nozaki*[4], *Tahei Tahara*[1,2]*

[1]Molecular Spectroscopy Laboratory, RIKEN, 2-1 Hirosawa, Wako 351-0198, Japan

[2]Ultrafast Spectroscopy Research Team, RIKEN Center for Advanced Photonics (RAP), 2-1 Hirosawa, Wako 351-0198, Japan

[3]PRESTO, Japan Science and Technology Agency, 4-1-8 Honcho, Kawaguchi 332-0012, Japan

[4]Graduate School of Science and Engineering, University of Toyama, 3190 Gofuku, Toyama 930-8555, Japan

*Correspondence to: tahei@riken.jp

1. Broadband fluorescence up-conversion spectroscopy of $K[Au(CN)_2]$ aqueous solutions

In order to complement the time-resolved absorption and TR-ISRS data, we carried out broadband fluorescence up-conversion measurements of $K[Au(CN)_2]$ aqueous solutions. Because this technique selectively monitors fluorescent excited states (e.g., S_1), it provides unambiguous information about their dynamics. Fig. S1a shows femtosecond time-resolved fluorescence spectra of the 0.3 M $K[Au(CN)_2]$ aqueous solution, measured with photoexcitation at 310 nm. Immediately after photoexcitation (0 ps), a broad emission spectrum having a maximum at around 370 nm shows up. (Note that a shoulder-like feature at around 350 nm denoted by the asterisk is due to the Raman signal of water.) The emission signal almost disappears by ~10 ps, with apparent red shift of the spectrum on the picosecond time scale. Because the time scale of the observed emission decay is much shorter than the phosphorescence lifetimes of the $[Au(CN)_2^-]$ oligomers (1.6 ns for the trimer, 27 ns for the tetramer, etc.),[1-2] the observed emission signal is attributable to the fluorescence of the $[Au(CN)_2^-]$ oligomers. Fig. S1b shows temporal profiles of the fluorescence intensity at selected wavelengths. The fluorescence in the short wavelength range (339 nm and 348 nm) mostly exhibits fast decays, being consistent with the previous up-conversion data at 350 nm (SI in ref. 1). On the other hand, the present measurement covering a wide emission wavelength range clearly reveals that the fluorescence decay is significantly different, depending on the monitored wavelength. Actually, at the emission wavelength of 360 nm, it is clear that the fluorescence decay consists of the fast and slow components with time constants of 0.38 ± 0.04 ps and 2.6 ± 0.04 ps, respectively, indicating the existence of multiple fluorescent species.

To identify these fast and slow fluorescent species, we evaluated relative contribution of each component in the fluorescence spectrum obtained immediately after photoexcitation, and examined how it changes with the concentration. Because the fast species decays with the 0.38-ps time constant and completely disappears by 2 ps, the spectrum at 2 ps is attributable solely to the slow species, yielding the

spectrum of the slow species (F_{slow}, green curve, Fig. S1c). On the other hand, the spectrum at 0.5 ps involves the contributions from both the fast and slow species. As shown in Fig. S1c, the 2-ps spectrum nicely matches the 0.5-ps spectrum in its red side region when it is scaled, which indicates that the red tail of the time-resolved fluorescence spectra is dominated by the slow species. Therefore, the scaled 2-ps spectrum can be regarded as the spectral contribution of the slow species contained in the 0.5-ps spectrum (F'_{slow}, yellow curve, Fig. S1c). Thus, the spectrum of the fast species (F_{fast}) is obtained by subtracting the F'_{slow} spectrum from the 0.5-ps spectrum, as shown with the blue curve in Fig. S1c. This spectral decomposition reveals that the fast and slow species exhibit their spectral maxima at around 350 nm and 370 nm, respectively. Then, we performed the same spectral decomposition also for the femtosecond time-resolved fluorescence data obtained for the 0.2 M $K[Au(CN)_2]$ aqueous solution, using the F_{slow} spectrum obtained from the 0.3-M data. The resultant F_{fast} and F'_{slow} spectra of the 0.2-M data are compared with those obtained from the 0.3-M data in Fig. S1d, after normalizing the peak intensities of the two F_{fast} spectra while keeping the F'_{slow} / F_{fast} ratio of each sample intact. This comparison clearly shows that the F'_{slow} / F_{fast} ratio of the 0.2-M solution is significantly smaller than that of the 0.3-M solution. These results clearly demonstrate that the two fluorescent species arise from different oligomers, i.e., the trimer and tetramer that co-exist in the solution, and that the fluorescence lifetimes (i.e., S_1 lifetimes) of the trimer and tetramer are 0.38 ps and 2.6 ps, respectively.

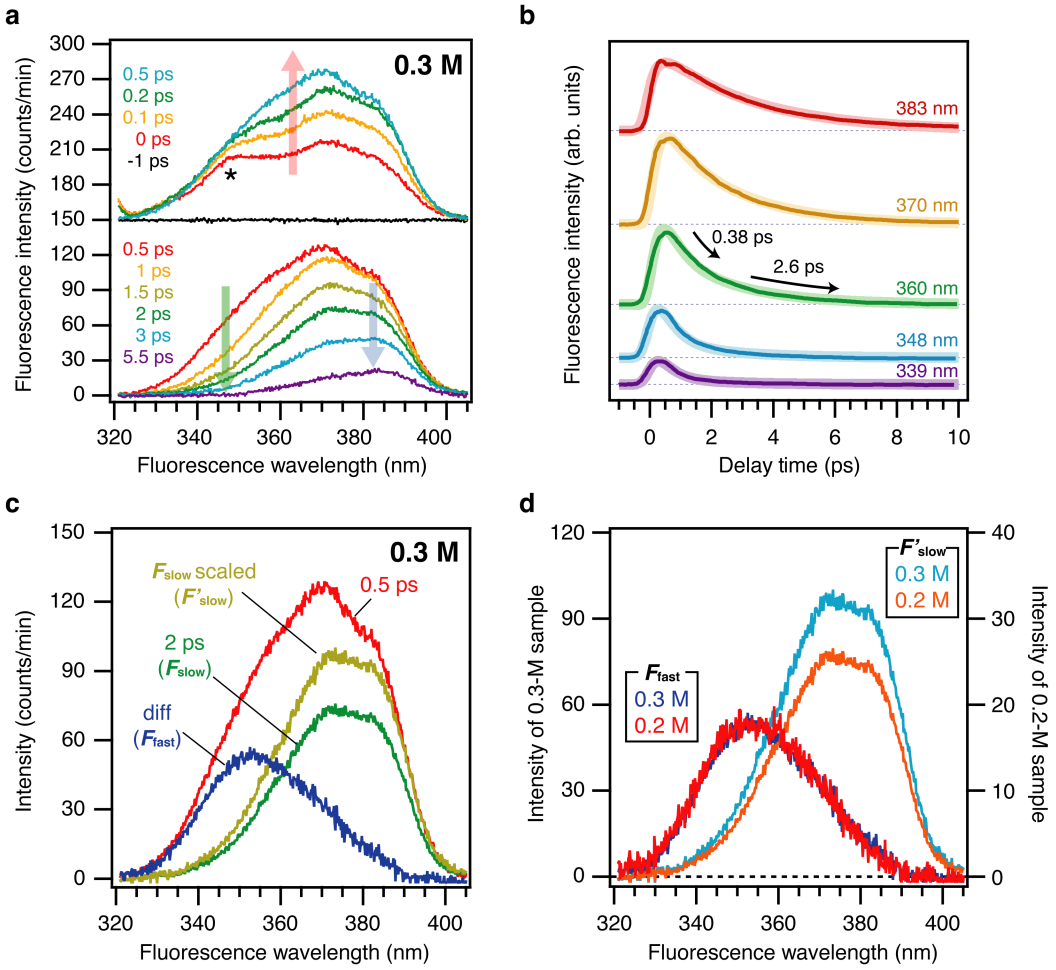

Figure S1. (a) Femtosecond time-resolved fluorescence spectra of the 0.3 M $K[Au(CN)_2]$ aqueous solution. Shoulder-like feature denoted by the asterisk is due to the Raman signal of water. Note that the spectral intensity above 385 nm is damped by the band-pass filter used for the measurement, so that the fluorescence spectrum may extend beyond 400 nm. (b) Temporal profiles of the time-resolved fluorescence signal at selected wavelengths. (c) Spectral decomposition of the time-resolved spectrum. The 0.5-ps spectrum consists of the fast (0.38 ps) and slow (2.6 ps) components. The spectrum of the fast component is obtained by subtracting the spectrum at 2 ps, i.e., the spectrum of the slow component (F_{slow}), from the 0.5-ps spectrum with appropriate scaling. (d) Comparison of the F_{fast} and F'_{slow} spectra obtained for the 0.3-M and 0.2-M solutions. Note that the 0.3- and 0.2-M data are normalized with the peak intensity of F_{fast} while keeping the F'_{slow} / F_{fast} ratio of each sample intact.

2. Ground-state Raman vibration of the $[Au(CN)_2^-]$ trimer

In the present study, we ruled out the contribution of the ground-state Raman signal in the TR-ISRS data. This is because we do not observe any oscillatory feature in the negative ΔT delay data, and the frequency of the Au-Au breathing vibration of the S_0 $[Au(CN)_2^-]$ trimer is different from any of those observed in the TR-ISRS data. Although the ground-state Raman-active vibration of the $[Au(CN)_2^-]$ trimer was not reported before, it was observed by resonant impulsive stimulated Raman process, as detailed in the following.

Fig. S2a shows the transient absorption data of the 0.31 M $K[Au(CN)_2]$ aqueous solution in the ultraviolet region obtained with 310-nm photoexcitation. The data exhibit the intense excited-state absorption (ESA) signal in the 320-360 nm region as well as the ground-state bleaching (GSB) signal in the <305-nm region. The temporal profile of the signal averaged over the GSB region (295-302 nm) is shown in Fig. S2b, and it clearly shows a very low frequency oscillatory feature (approximately 30 cm^{-1}). Such a low-frequency oscillation was not observed in the previous transient absorption experiments of the 0.28 M solution that monitored the ESA signal in the visible region.[1] Therefore, the observed low-frequency oscillation is highly likely due to the Au-Au breathing vibration of the $[Au(CN)_2^-]$ trimer in the ground state, which is induced by the resonant impulsive stimulated Raman process. (We note that the Au-Au breathing vibration with a similar frequency (36 cm^{-1}) was previously observed for the binuclear Au(I) complex having a comparable Au-Au distance (~3.5 Å).)[3] As shown in the lower panel of Fig. S2b, a similar oscillatory feature is also observed for the 0.1 M solution, so that the low-frequency oscillation should not be assigned to the larger oligomer, i.e., the tetramer. Unfortunately, the detailed quantitative analysis of this oscillatory feature is hampered by the rapid dephasing, interference by intense coherent artifact around the time origin, and difficulty in the estimation (and subtraction) of the early population dynamics (<1 ps). Nevertheless, it is clear that its frequency is very different from those observed in the

TR-ISRS data. Therefore, it is safely concluded that the contribution of the ground-state Raman signal of the $[Au(CN)_2^-]$ trimer is negligible in the TR-ISRS data shown in the main text.

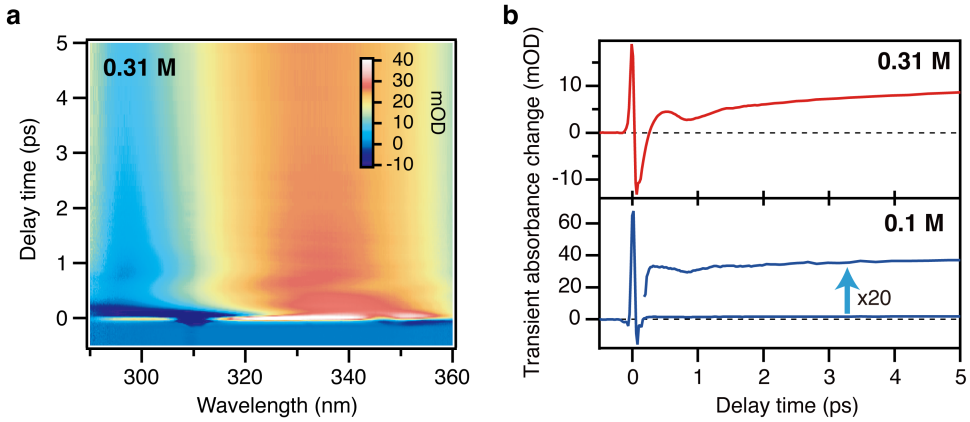

Figure S2. (a) Transient absorption data of the 0.31 M $K[Au(CN)_2]$ aqueous solution obtained upon 310-nm photoexcitation. (b) Temporal profile of the transient absorption signal averaged over the 295-302-nm region (red). The data obtained for the 0.1 M solution is also shown for comparison (blue). The pump pulse energy was 200 nJ for the 0.31 M data and 500 nJ for the 0.1 M data.

3. Concentration dependence of the Au-Au breathing vibration frequency of the T_1 $[Au(CN)_2^-]$ trimer

Comparison of the 0.29 M and 0.1 M TR-ISRS data (Fig. 3c and Fig. 4a in the main text) not only points to the significant contribution of the larger oligomer in the 0.29 M data, but also the noticeable frequency difference of the Au-Au breathing vibration of the T_1 trimer at different concentrations (~92 cm^{-1} for 0.1 M and ~99 cm^{-1} for 0.29 M, at ΔT = 10 ps). This behavior was further examined at other concentrations. Fig. S3a shows the temporal change of the frequency of the Au-Au breathing vibration, measured at various concentrations. At the early ΔT delays, the frequency is almost the same for all the concentrations (~87 cm^{-1}). On the other hand, the frequency at the late ΔT delay times, at which the T_1 trimer takes the linear-staggered structure, increases as the concentration is increased, suggesting the

tighter Au-Au bond formation at the higher concentration. This observation can be understood in terms of the screening of the electrostatic repulsions between the cyano groups by the co-existing K^+ ions in the solution. Indeed, this interpretation is supported by the ionic strength dependence of the Au-Au breathing frequency examined with keeping the $K[Au(CN)_2]$ concentration same, in which increase in the frequency was observed with the increase in the ionic strength (Fig. S3b). It is worth noting that this effect is seen only in the linear-staggered structure that appears in the late ΔT delay time region but negligible in the early ΔT region. This is presumably because the cyano groups do not have a specific relative orientation in the bent structure and do not significantly interact with one another. The stabilization by K^+ gradually comes into effect as the bent-to-linear structural change proceeds and the cyano groups start to interact each other.

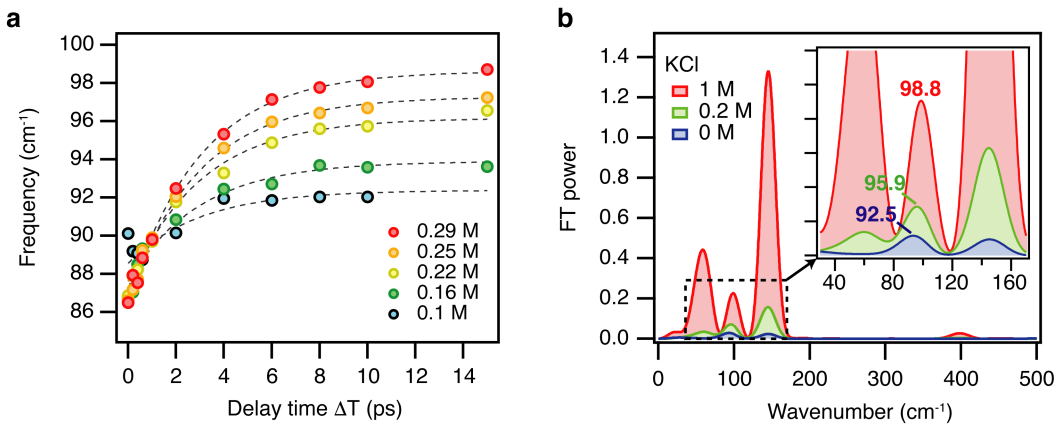

Figure S3. (a) Temporal profiles of the Au-Au breathing frequency of the T_1 $[Au(CN)_2^-]$ trimer, obtained for the $K[Au(CN)_2]$ aqueous solutions of various concentrations. Gray broken lines denote the best fit to the data using the 3-ps time constant. (b) Fourier transform power spectra of the oscillatory component of the TR-ISRS signals obtained for the 0.11 M $K[Au(CN)_2]$ aqueous solutions with and without additional KCl. The ΔT delay time was set at 15 ps.

References

1. Iwamura, M.; Nozaki, K.; Takeuchi, S.; Tahara, T., Real-Time Observation of Tight Au–Au Bond Formation and Relevant Coherent Motion Upon Photoexcitation of $[Au(CN)_2^-]$ Oligomers. *J. Am. Chem. Soc.* **2013,** *135* (2), 538-541.
2. Iwamura, M.; Wakabayashi, R.; Maeba, J.; Nozaki, K.; Takeuchi, S.; Tahara, T., Coherent Vibration and Ultrafast Dynamics Upon Bond Formation in Excited Dimers of an Au(I) Complex. *Phys. Chem. Chem. Phys.* **2016,** *18* (7), 5103-5107.
3. Perreault, D.; Drouin, M.; Michel, A.; Miskowski, V. M.; Schaefer, W. P.; Harvey, P. D., Silver and Gold Dimers. Crystal and Molecular Structure of $Ag_2(dmpm)_2Br_2$ and $[Au_2(dmpm)_2](PF_6)_2$ and Relation between Metal-Metal Force Constants and Metal-Metal Separations. *Inorg. Chem.* **1992,** *31* (4), 695-702.